

ANALYSIS AND SIMULATION OF A CASCADED SHUNT ACTIVE POWER FILTER FOR ELECTRIC POWER SYSTEM

Suman Thummalapalli¹, R. Jagadeesh Nethra², M. Venkateswara Reddy³

*¹PG Student, ²Assistant Professor, ³Associate Professor
Department of EEE, Vikas Group of Institutions, Nunna, Vijayawada, AP, (India)*

ABSTRACT

Introducing APF technology into the aircraft power system to improve the quality and reliability of the system becomes a preferable solution. Shunt active power filters are a viable solution for power quality enhancement, in order to comply with the standard recommendations. It is not easy for the power-quality characteristics of the system to be in compliance with the harmonic standards by using traditional method to compensate the harmonics introduced by the nonlinear load. . The three stage H-bridge cascaded inverter is selected for the aeronautical APF (AAPF). The control levels are increased to improve the performance of APF. The increased control level can increase the aircraft power system power quality and reliability. The global frame work and operation principal of proposed AAPF are presented in detail. Source current direct control strategy and cascaded inverter topology is applied in the proposed AAPF. The power quality characteristics of the conventional system are not up to level. Performance characteristics of EPS with conventional systems are not preferable.

Index Terms—Aeronautical active power filter (APF) (AAPF), cascaded multilevel inverter

I.INTRODUCTION

The latest research about civil aircraft systems has moved towards the increasing use of electric power in place of other conventional sources like mechanical, hydraulic, pneumatic power. This technological trend is known as the More Electric Aircraft. Recent advances in the areas of power electronics, electric devices, control electronics, and microprocessors have allowed fast improvements in the performance of aircraft electrical systems. The use of more electric power brings significant advantages for the operation of the whole system. These advantages are listed here. Advantages of the increasing use of electric power in the aircraft system:

- optimization of the performance
- optimization of the life cycle cost
- reduction of weight and size of the equipment
- increased reliability

Important changes are brought important changes are brought to the aircraft electrical system due to the increasing use of electric power on board. These changes are listed below Consequences of the increasing use of electric power on the aircraft electrical system:

- more electrical loads
- more complex topology of the electrical network

- In this paper, a high-performance aircraft APF is proposed. Differently from traditional open-loop control strategy, the proposed aeronautical APF (AAPF) works in a close-loop way. Good power quality of the EPS is achieved by using the novel AAPF. Furthermore, in order to improve the dynamic performance of the load response, a feed forward path of the load current is added. Based on the modeling and analysis of the close-loop system, the operation principle of the feed forward compensation path is revealed. Meanwhile, the control method of the cascaded-inverter-based AAPF is proposed. The operation principle containing the overall voltage control and voltage-balance control is given. Simulation results under different fundamental frequencies and load conditions are given. In order to verify the aforementioned analysis and compensation performance of the proposed AAPF, an aircraft APF system with a 7.2-kVA load power is built and tested in the laboratory.

27 | Page

2.2. Source Current Direct Control

In this paper, the close-loop control named as source current direct control is applied as the main control strategy of the proposed AAPF. The source current direct control is proposed in [16] by Wu and Jou. The basic system diagram of the close loop control scheme is given in Fig. 1. This control strategy operates as follows: The dc-link voltage is sent to the voltage regulator, and the output of the regulator is sent to the multiplier as well as a synchronous sine wave which is detected from the phase voltage. The output of the multiplier is sent to the current regulator, being the source current reference. The output of the current regulator will be sent to the modulator to generate the pulse width modulation waveforms. Fig. 2 gives the equivalent control model of this compensation strategy. As shown in Fig. 2, the source current reference of the source current direct control comes from the variation of the dc-link voltage. Here, $G_v(s)$ corresponds to the transfer function of the voltage controller; K_f is the dc-link voltage detection coefficient.

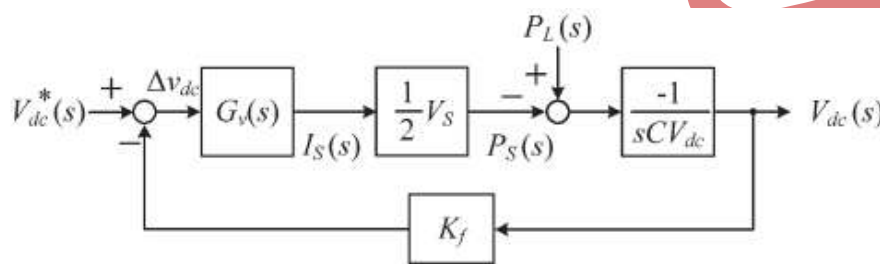


Fig. 2. Model for active power analysis.

2.3. Load Current Feed forward Compensation

As Fig. 2 illustrates, load power $P_L(s)$ works as a disturbance factor on the APF system. The transfer function between $P_L(s)$ and $\Delta V_{dc}(s)$ is

$$\Phi_{en}(s) = \frac{\Delta V_{dc}(s)}{P_L(s)} = \frac{\frac{1}{sCV_{dc}} K_f}{1 + G_v(s) \cdot \frac{1}{2} V_s \cdot \frac{1}{sCV_{dc}} \cdot K_f} \quad (1)$$

The transfer function between $I_L(s)$ and $I^*S(s)$ is

$$\begin{aligned} H_{iL}(s) &= \frac{I_s^*(s)}{I_L(s)} = \frac{\Delta V_{dc}(s) G_v(s)}{P_L(s) / (\frac{1}{2} V_s)} = \Phi_{en}(s) \cdot \frac{G_v(s)}{\frac{1}{2} V_s} \\ &= \frac{G_v(s) \cdot \frac{1}{2} V_s \cdot \frac{1}{sCV_{dc}} K_f}{s + G_v(s) \cdot \frac{1}{2} V_s \cdot \frac{1}{sCV_{dc}} K_f} = \frac{A \cdot G_v(s)}{s + A \cdot G_v(s)} \end{aligned} \quad (2)$$

Where $A = V_s K_f / (2CV_{dc})$.

$H_{iL}(s) |_{f=50}$ shows the dynamic speed of the current reference responding to the load power's change at fundamental frequency. Generally speaking, high dynamic response is required for an APF system, meaning that a higher value of $H_{iL}(s) |_{f=50}$ is desired. However, $H_{iL}(s)$ is sensitive to many other factors, i.e., voltage controller, line voltage, dc-link voltage, dc-link capacitor, and voltage detection coefficient. Fig. 3 shows the bode diagram of $H_{iL}(s)$ in different voltage controller and coefficient A. For an APF system applied in a 220-V/50-Hz application, coefficient A corresponds to 0.14 when the dc-link voltage is 800 V, dc-link voltage detection coefficient K_f is 0.005, and the dc-link capacitor is 6800μF. It is hard to design a voltage controller to derive a high value for $H_{iL}(s) |_{f=50}$ at 50 Hz in such a low value of A. In the aircraft EPS, the phase voltage is only 115 V, leading A to be 0.2 when the dc-link voltage is 600 V, dc-link voltage detection coefficient K_f is

0.005, and the dc-link capacitor is 3300 μ F. It means that poor dynamic respond is derived in both applications. In order to improve the dynamic speed responding to the load's change, a feed forward compensation path is added to weaken the disturbance effect of the load current, as shown in Fig. 3. Here, $F(s)$ is the transfer function of the low-pass filter (LPF) which extracts the fundamental components of the load currents

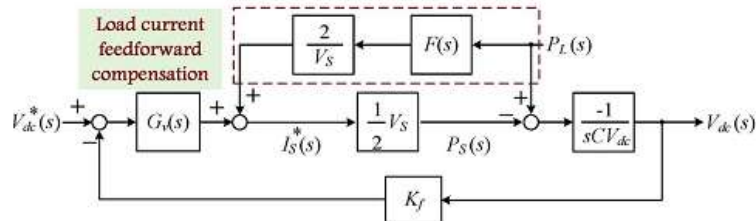


Fig.3.Disturbance compensation-based closed-loop control.

$$F(s) = \frac{\omega_0^2}{s^2 + \sqrt{2}\omega_0 s + \omega_0^2} \quad (3)$$

Here, $\omega_0=2\pi f_c$ is the cutoff angular frequency of the LPF. After the fundamental of the load current is feed forward, the transfer function between $I_L(s)$ and $I_s(s)$ becomes After the load current is feed forward, the magnitude of $|H_{IL}(s)|_{f=50}$ gets increased. However, the selection of f_c plays an important role to $H_{IL}(s)$; usually, f_c should be larger than the fundamental frequency.

III. CONTROL METHOD OF THE CASCADED-INVERTER-BASED AAPF

3.1. Discussion and Demonstration on the Power Stage of AAPF

A shunt APF acts as a controlled harmonic current source, injecting current which is inverse equivalent to the load harmonic. In the 400-Hz aircraft EPS, frequencies of the 11th and 13th harmonics reach as high as 4.4 and 5.2 kHz. How to draw a high-frequency harmonic current accurately is a key issue of developing AAPF.

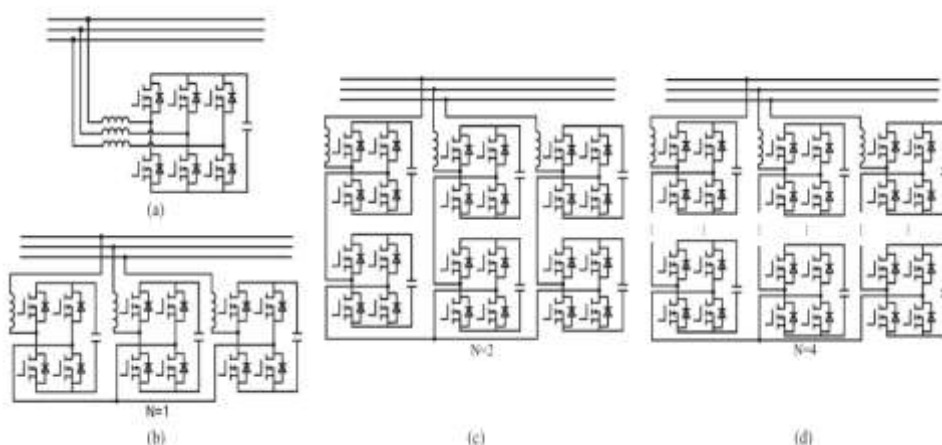


Fig. 4. Four possible solutions of AAPF. (a) Three-leg-inverter-based APF. (b) H-bridge-based APF. (c) Two H-bridge cascaded APF. (d) Four H-bridge cascaded APF.

Figure4 shows four possible solutions of AAPF: the three leg-inverter-based APF, the H-bridge-based APF, the two

H-bridge cascaded APF, and the four H-bridge cascaded APF. Comparative study of these solutions is taken as follows. For the first solution, in order to achieve good current tracking performance in 400-Hz system, the switching frequencies of AAPF are selected as 60, 120, and 240 kHz, and the dc-link voltage is adopted as 400 V. For the second solution, considering the “double equivalent switching frequency effect” of the carrier phase shift (CPS) PWM modulation the switching frequencies of AAPF are selected as 30, 60, and 120 kHz, and the dc-link voltage is adopted as 300 V. Meanwhile, the same equivalent switching frequency means almost the same current tracking performance and almost the same bandwidth of AAPF. The power switches in Table I are all from International Rectifier (IR) Corporations with the current rating near 24 A. The switching losses and conductive losses of the power MOSFET could be evaluated by using the switching loss estimation method used as follows:

$$P_{SW} = \frac{1}{2} I_D V_D (t_{OFF} + t_{ON}) f_{sw} + \frac{1}{2} C_{OSS} V_D^2 f_{sw} \quad (4)$$

$$P_{con} = \bar{I}_{RMS}^2 R_{ds(on)} D + V_{DF} I_D (1 - D) \quad (5)$$

Here, PSW and P concor respond to switching loss and conductive loss, and ID, VD, and fsw are the drain current, bus voltage, and switching frequency, while tON and tOOF Fare the power MOSFET turn-on and turnoff times, respectively. COSSRs (on) are the output capacitance and the on-resistance of the power MOSFET while VDF is the forward voltage drop of the reverse parallel diode of the power MOSFET.

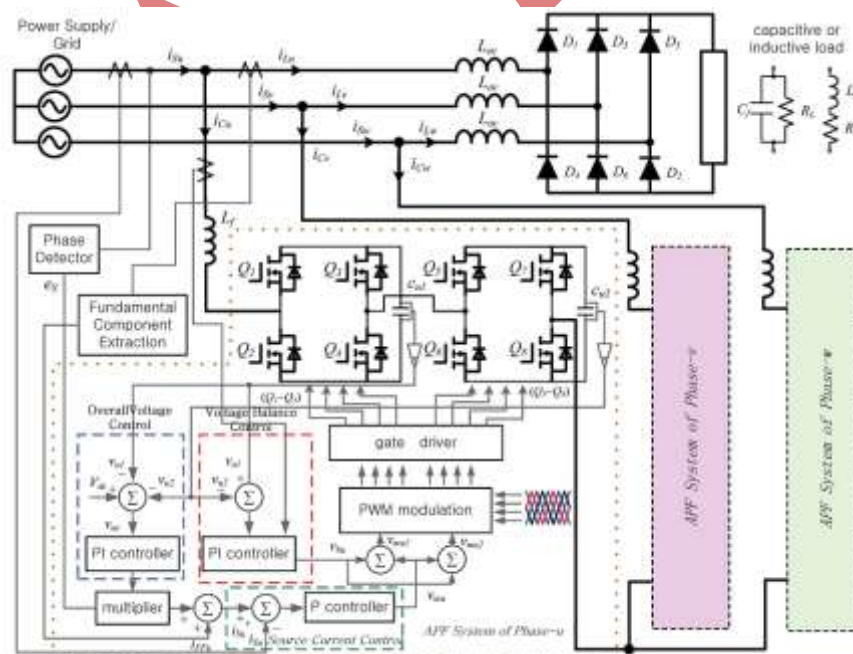


Fig. 5. System diagram of the proposed AAPF.

In this paper, the two H-bridge cascaded APF is selected as the power stage configuration of the AAPF, both for the accepted small power loss and reliability (as shown in Fig.5). The switching frequency is selected as 30 kHz,

so the ac voltage of each cluster becomes a five-level line-to neutral PWM waveform with the lowest harmonic sideband centered at 120 kHz ($= 30 \text{ kHz} \times 2 \times 2$). Maintenance of the voltage balance of the capacitors is critical to the safe operation of the H-bridge-based AAPF. The voltage-balance control of the floating dc capacitors can be divided into the following:

- 1) Clustered overall control.
- 2) Balancing control.

3.2. Clustered Overall Control

In the cluster overall voltage control loop, sums of the capacitor voltages in each cluster (for example: v_{u1} and v_{u2} for phase-u) are the control target. This cluster overall control yields the u-phase clustered overall voltage signal v_{ou} from the dc capacitor voltage reference v_{dc} , the dc capacitor voltages of the u-phase cluster v_{u1}, v_{u2} , and the synchronous sine wave e_{Su} (as shown in Fig. 6). Furthermore, this voltage control scheme could be expanded to the NH-bridge cascaded inverter topology. Here, N corresponds to the number of cascaded converter units. One obvious advantage of this control scheme is that the final compensation performance would not get worse when one or more cascaded units stop working.

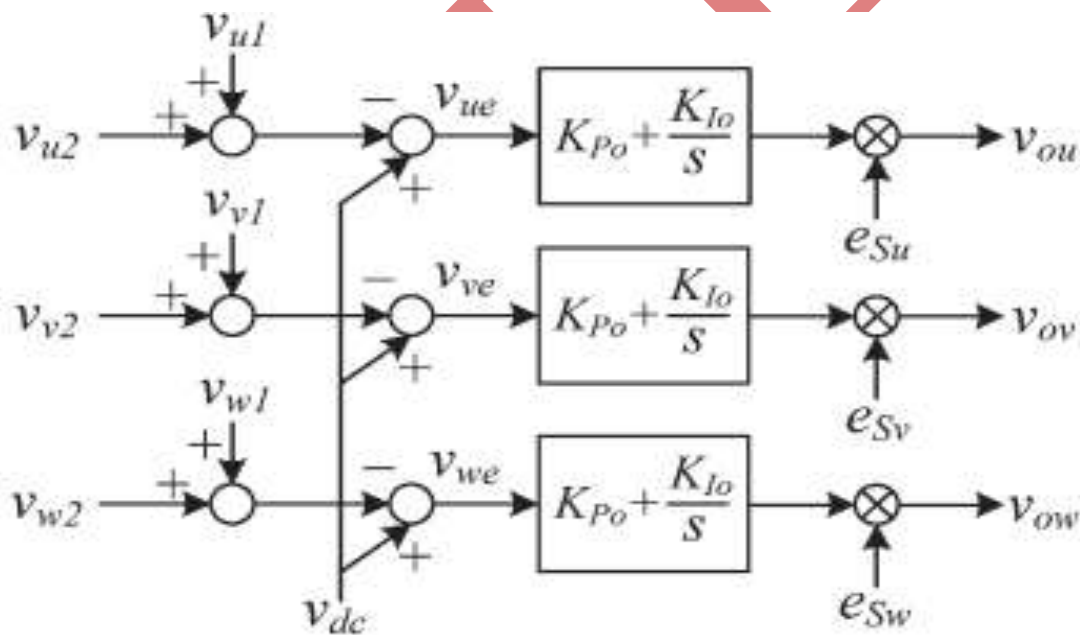


Fig. 6. Control diagram of the cluster overall control.

The remaining cascaded units would share the dc-link voltage of the fault one. This voltage control scheme can increase the fault toleration and reliability of the AAPF system.

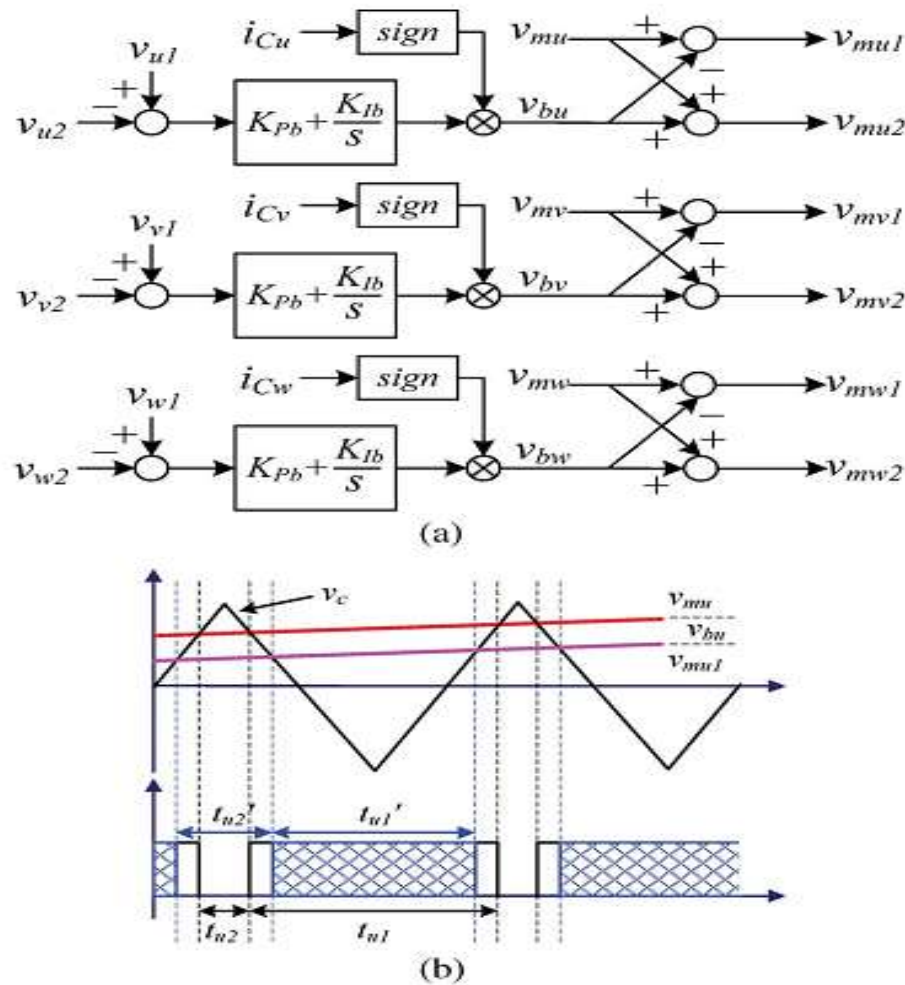


Fig. 7. Operation principle of voltage-balance control. (a) Control diagram. (b) Regulation procedure.

3.3. Balancing Control

As Fig. 7(a) shows, the balancing control yields a balance control signal v_{bn} ($n=u, v, w$) to make the voltage of the capacitors in each cluster balanced. The individual balance control yields two modulation waves v_{mn1} and v_{mn2} from the origin modulation wave v_m and the dc capacitor voltages of each cluster v_{n1} , v_{n2} . In the CPS PWM modulation, PWM signals for Q1, Q2 and Q3, Q4 are modulated by v_{mn1} , while PWM signals for Q5, Q6 and Q7, Q8 are modulated by v_{mn2} . The current direction and the switch combination define the charging or discharging of the each particular capacitor of the dc link. Depending on the current direction and needed charging or discharging process, the voltage signal v_{bu} should be added or subtracted to/from the modulating signal. For the upper cascaded unit, the input power decreases when the duty cycles of Q1 and Q4 decrease, resulting in the dc-link voltage v_{u1} being reduced. Similarly, the dc-link voltage of the lower cascaded unit v_{u2} will get increased. The voltage balance is therefore achieved. Take the phase-u cluster for example to show the regulation procedure of voltage-balance control [as shown in Fig. 7(b)]. In the steady state, the modulation wave of bridge 1 (composed of Q1 and Q2) is v_{μ} , and the conduct times of Q1 and Q2 are t_{u1} and t_{u2} , respectively. When the situation $v_{u1} > v_{u2}$ happens, a positive balance control voltage signal v_{bu} is obtained under the regulator's action. As Fig. 7(a) shows, the final modulation wave for Q1 and Q2 is the sum of v_{μ} and $-v_{bu}$, which becomes $v_{\mu1}$ after regulation. Therefore, the conduction times of Q1 and Q2 turn to

be t'_{u1} and t'_{u2} . As Fig. 7(b) illustrates, we could find that $t'_{u1} < t_{u1}$ and $t'_{u2} > t_{u2}$, which means that the duty cycle of Q1 decreased but the duty cycle of Q2 increased.

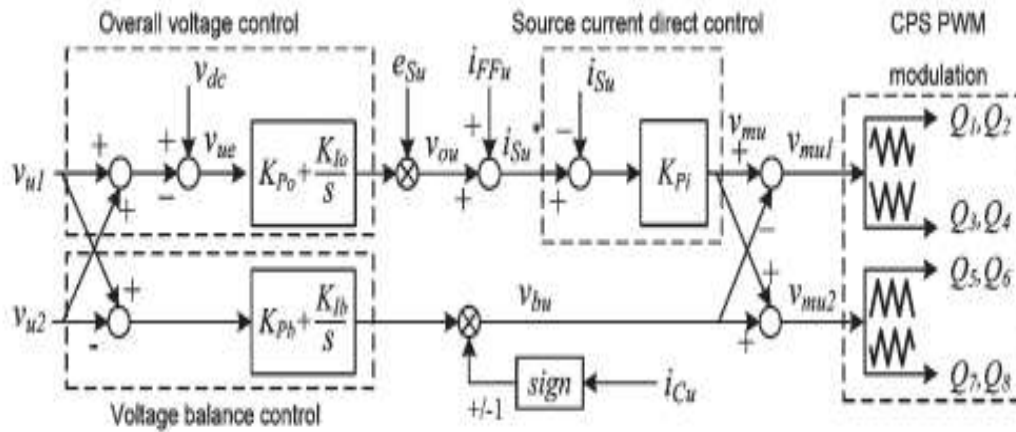


Fig. 8. Control diagram for phase-u of the proposed AAPF.

Meanwhile, the duty cycle of Q3 increased, and the duty cycle of Q4 decreased. The whole control diagram for phase-u of the proposed AAPF is given in Fig. 8, which contains the overall voltage control, voltage-balance control, load current feed forward compensation, and source current direct control.

IV. MATLAB/SIMULINK RESULTS

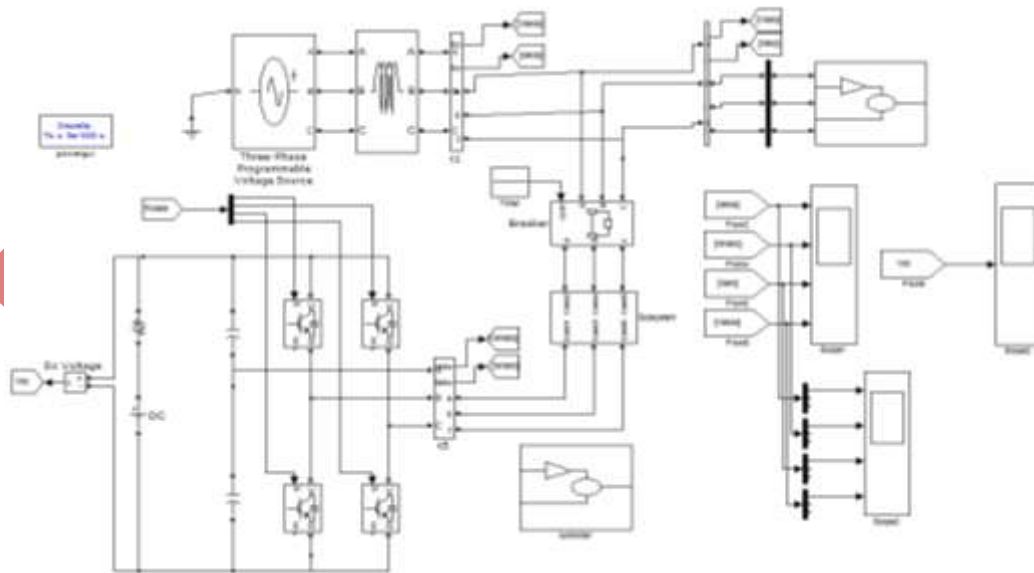


Fig. 9. Matlab/Simulink model of inductive load.

Figure9 shows the Matlab/Simulink model of inductive load.

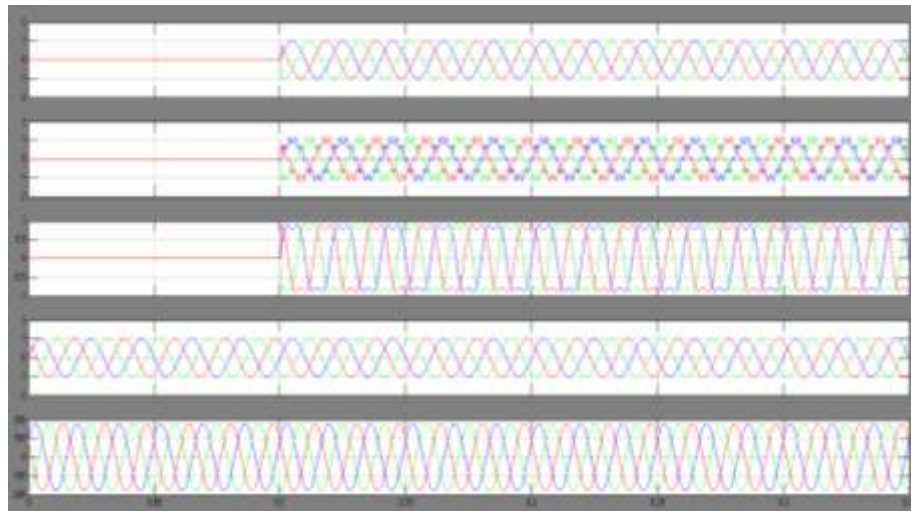


Fig. 10. Inductive load of sinusoidal phase voltage and distorted phase voltage.

Figure10 shows the inductive load of sinusoidal phase voltage and distorted phase voltage.

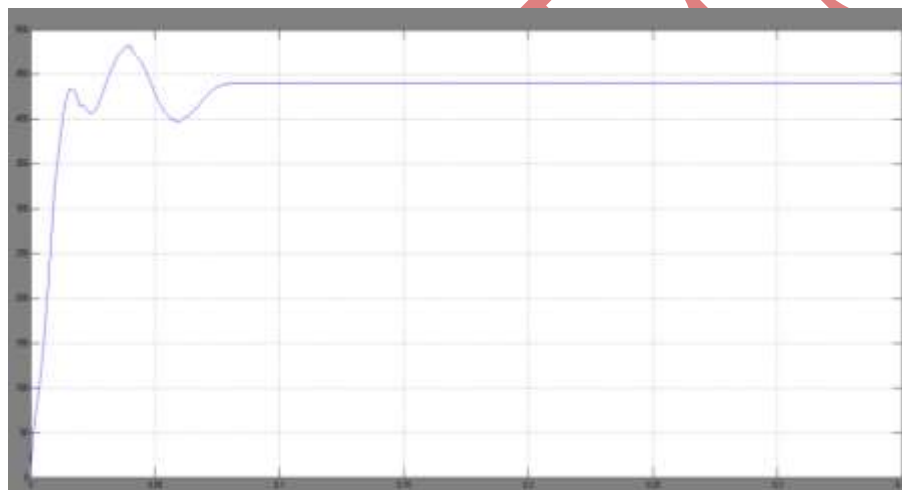


Fig. 11. DC capacitor voltage waveforms under loading.

Figure11 shows the DC capacitor voltage waveforms under loading.

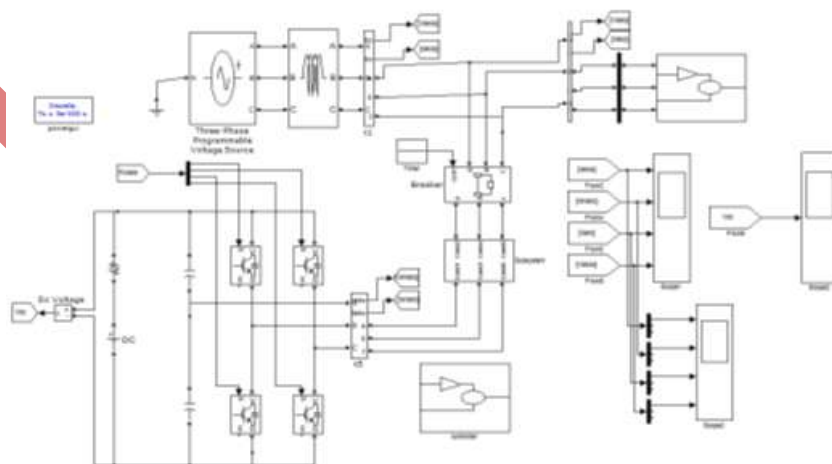


Fig. 12. Matlab/Simulink model of capacitive load

Figure12 shows the Matlab/Simulink model of capacitive load.

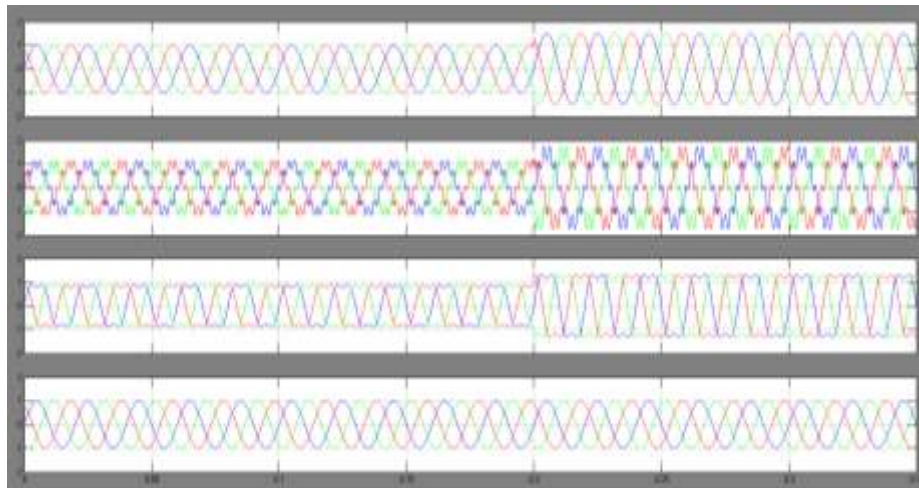


Fig. 13. Waveforms under loading.

Figure13 shows the waveforms under loading.

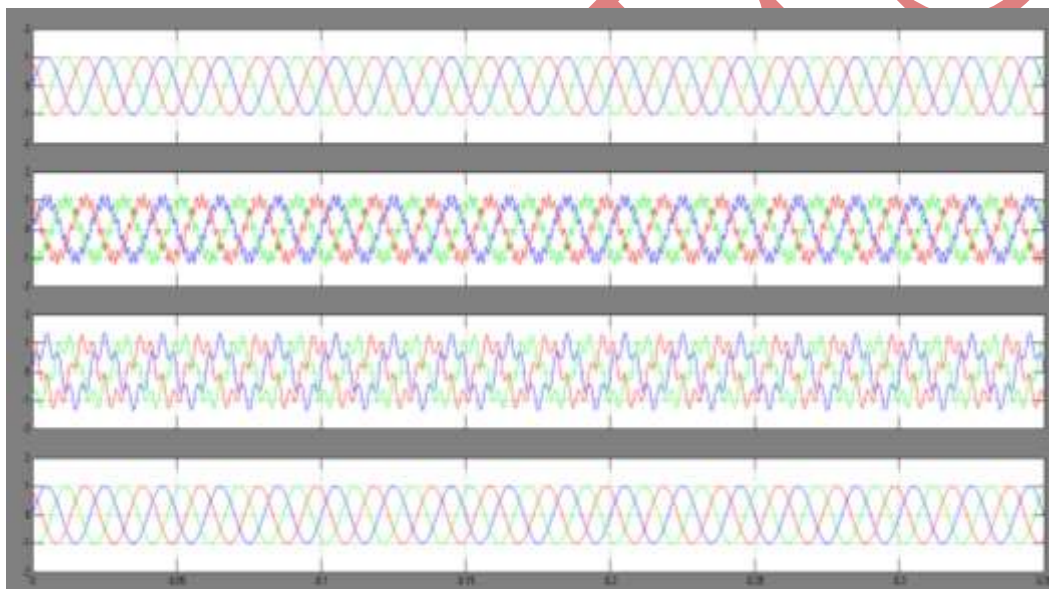


Fig. 14. Simulation waveforms of AAPF under variable-frequency EPS.

Figure14 shows the Simulation waveforms of AAPF under variable-frequency EPS.

V.CONCLUSION

APF technology is a useful method to resolve the power quality issues of the modern aircraft EPS. In this paper, a load current feed forward compensation method for the source current direct control-based AAPF has been proposed. The corresponding system control strategy of the cascaded-inverter based active filter system is shown. The corresponding system seven level control strategy of the cascaded-inverter based active filter system is shown. The simulation results are shown the good compensation behavior for various kinds of load condition and the excellent dynamic performance of proposed control method. Compensation performance of the proposed AAPF, simulated waveforms using the “Simulink” software package of “Matlab” is verified.

REFERENCES

- [1] J. A. Rosero, J. A. Ortega, E. Aldabas, and L. Romeral, "Moving towards a more electric aircraft," *IEEE Aerosp. Electron. Syst. Mag.*, vol. 22, no. 3, pp. 3–9, Mar. 2007.
- [2] A. Hamadi, S. Rahmani, and K. Al-Haddad, "A hybrid passive filter configuration for VAR control and harmonic compensation," *IEEE Trans. Ind. Electron.*, vol. 57, no. 7, pp. 2419–2434, Jul. 2010.
- [3] A. Varschavsky, J. Dixon, M. Rotella, and L. Moran, "Cascaded nine-level inverter for hybrid-series active power filter, using industrial controller," *IEEE Trans. Ind. Electron.*, vol. 57, no. 8, pp. 2761–2767, Aug. 2010.
- [4] A. Luo, X. Xu, L. Fang, H. Fang, J. Wu, and C. Wu, "Feedback– feed forward PI-type iterative learning control strategy for hybrid active power filter with injection circuit," *IEEE Trans. Ind. Electron.*, vol. 57, no. 11, pp. 3767–3779, Nov. 2010.
- [5] S. Rahmani, N. Mendalek, and K. Al-Haddad, "Experimental design of a nonlinear control technique for three phase shunt active power filter," *IEEE Trans. Ind. Electron.*, vol. 57, no. 10, pp. 3364–3375, Oct. 2010.
- [6] B. Singh and J. Solanki, "An implementation of an adaptive control algorithm for a three-phase shunt active filter," *IEEE Trans. Ind. Electron.*, vol. 56, no. 8, pp. 2811–2820, Aug. 2009.
- [7] A. Bhattacharya and C. Chakraborty, "A shunt active power filter with enhanced performance using ANN-based predictive and adaptive controllers," *IEEE Trans. Ind. Electron.*, vol. 58, no. 2, pp. 421–428, Feb. 2011.
- [8] D. Ganthony and C. M. Bingham, "Integrated series active filter for aerospace flight control surface actuation," in *Proc. EPE*, 2007, pp. 1–9.
- [9] E. Lavopa, E. Summer, P. Zanchetta, C. Ladisa, and F. Cupertimo, "Real time estimation of fundamental frequency and harmonics for active power filters applications in aircraft electrical systems," in *Proc. EPE*, 2007, pp. 4220–4229.
- [10] E. Lavopa, M. Summer, P. Zanchetta, C. Ladisa, and F. Cupertimo, "Real-time estimation of fundamental frequency and harmonics for active power filters applications in aircraft electrical systems," *IEEE Trans. Ind. Electron.*, vol. 56, no. 8, pp. 2875–2884, Aug. 2009.
- [11] M. Odavic, P. Zanchetta, and M. Summer, "A low switching frequency high bandwidth current control for active shunt power filter in aircrafts power networks," in *Proc. IEEE IECON*, 2007, pp. 1863–1868.